Thermochimica Acta 510 (2010) 103–112

Contents lists available at ScienceDirect

Thermochimica Acta

journal homepage: www.elsevier.com/locate/tca

Non-isothermal crystallization kinetic of poly(ethylene terephthalate)/fumed silica (PET/SiO_2) prepared by in situ polymerization

G. Antoniadis [a], K.M. Paraskevopoulos [a], D. Bikiaris [b], K. Chrissafis [a,*]

[a] School of Physics, Solid State Physics Department, Aristotle University of Thessaloniki, 54124 Thessaloniki, Greece
[b] Department of Chemistry, Aristotle University of Thessaloniki, 54124 Thessaloniki, Greece

ARTICLE INFO

Article history:
Received 27 April 2010
Received in revised form 1 July 2010
Accepted 2 July 2010
Available online 29 July 2010

Keywords:
Poly(ethylene terephthalate)
Fumed silica
Activation energy
Nanocomposites
Crystallization

ABSTRACT

A number of poly(ethylene terephthalate) (PET) nanocomposites were prepared by in situ polymerization using different amounts (0.5, 1, 2, 3 and 4 wt%) of fumed silica (SiO_2). The polymerization of PET was carried out by the two-stage melt polycondensation method. From DSC studies it was found that the melting point of the nanocomposites was shifted slightly to higher temperatures by the addition of SiO_2 till 3 wt% while for PET–4 wt% SiO_2 nanocomposite the melting point was reduced. As the amount of SiO_2 was increased the crystallization became faster, and there was, also, a shifting of the temperature of the crystallization peak to higher values, this being evidence that SiO_2 can act as nucleating agent. At higher content (3 and 4 wt%) the temperature of the crystallization peak is lower than that of PET–2 wt% SiO_2 due to the formation of crosslinked macromolecules. The activation energy is calculated with the Friedman's method. PET/SiO_2 samples present lower activation energy compared to that of neat PET, except those of PET–4% SiO_2, in which the activation energy have a maximum value for $\alpha = 0.8$ probably due to the second crystallization peak. Extensive crystallization studies by using Avrami, Ozawa and Malek methods verified that PET and its nanocomposites must be crystallized by two mechanisms with different activation energies taking place in different degrees of crystallization.

1. Introduction

The investigation of the kinetics of polymer crystallization is significant both from the theoretical and practical point of view. The mechanism of the formation of fine structure during polymer crystallization has practical importance and it arises from the effect of crystallinity on both physical and chemical properties of polymer.

Poly(ethylene terephthalate) (PET) is a linear semi-crystalline thermoplastic polyester with excellent mechanical, physical, and chemical properties, including very good heat resistance, high stiffness and strength, and good dimensional stability. These properties make PET an attractive high performance polymer for engineering plastic applications in areas of electronics, transportation, construction, and consumer products. However, PET application as an engineering plastic for injection moulding is rather limited, due to its slow crystallization rate and large cycle time [1].

The first studies on the non-isothermal crystallization of PET were carried out in 1971 when Ozawa [2] proposed a new method to analyze data for the solidification of semi-crystalline polymers cooled at a constant cooling rate.

Crystallization process of PET has recently been reexamined due to the increasing theoretical and technological interest. Valev and Betchev [3] studied the crystallization thermodynamics and kinetics of amorphous PET fibers subjected to simultaneous thermal and mechanical treatments. They found that the Ozawa's model can be used for the qualitative description of the amorphous PET fibers crystallization.

In order to increase its performance, during last years, nanocomposites were prepared and studied, especially that containing silica nanoparticles (SiO_2). Fumed silica is a non-crystalline, fine-grain, low density and high surface area silica. Zheng and Wu [4] in their study have shown that nanosilica do not behave as a nucleating agent but rather retard the appearance of the microcrystalline phase that enhances spinnability. Liu et al. [5] have found that the addition of nanoparticles increases the crystallization temperature and the melting point of the polymer. Additionally, nanoparticles do not affect very much the process of pure PET synthesis. Yang et al. [6] demonstrated that it is possible to control the crystallization behavior of PET by inorganic nanoparticles. Wang et al. [7] studied the non-isothermal crystallization behavior of pristine PET and PET/clay nanocomposites with a differential scanning calorimeter (DSC), and found that the introduction of clay into PET matrix weakens the dependence of the non-isothermal crystallization exotherm peak temperatures on the cooling rates. Additionally, they verified that the absolute value of activation

* Corresponding author. Tel.: +30 2310 998188; fax: +30 2310 998188.
E-mail address: hrisafis@physics.auth.gr (K. Chrissafis).

0040-6031/$ – see front matter © 2010 Elsevier B.V. All rights reserved.
doi:10.1016/j.tca.2010.07.003

energy for PET is lower than that of PET/clay nanocomposites. Jeziorny [8] calculated the parameters that are characterizing the kinetics of non-isothermal crystallization on the basis of DSC thermograms and he concluded that, by changing the cooling rate, the morphology of the crystalline structure can be determined in a controlled manner as a result of the non-isothermal crystallization. Bikiaris et al. [9] found that solid-state polycondensation can act as a facile method to prepare poly(ethylene terephthalate)/silica (PET/SiO_2) nanocomposites with high molecular weight and an adjustable degree of branching or crosslinking. He et al. [10] prepared PET–SiO_2 nanocomposites by in situ method, and found that the PET crystallization rate increases significantly with increasing the silica content. The silica nanoparticles can act as an efficient nucleating agent to facilitate PET crystallization. Zhu et al. [11] presented a thorough study of the thermal behavior of the cryomilled PET/SiO_2 nanocomposites, and found that cryomilling resulted in amorphization of crystalline PET matrix and simultaneously, in the fracturing of molecular chains and the decrease of the molecular weight, and consequently, it is concluded that the SiO_2 particles have an additive milling effect. Ke et al. [12] investigated the nucleation, crystallization and dispersion behavior of silica particles in PET matrix and found that in non-isothermal crystallization, the crystallization activation energy for PET/silica nanocomposites was lower than that for PET while the nucleation rate of silica particles was increased with the decrease in size, the 35 nm SiO_2 particles producing most obvious nucleation effect.

However, as far as we know, there are no reports about the non-isothermal crystallization behavior of PET/SiO_2 nanocomposites, and for this reason in this study, we present an in depth examination of the crystallization kinetics of the mentioned nanocomposites, using differential scanning calorimetry.

2. Experimental

2.1. Materials

Dimethyl terephthalate (DMT) (99%), anhydrous 1,2-ethanediol (EG) (99%), antimony trioxide (Sb_2O_3) (98%) and triphenylphosphate (TPP) (95%) were obtained from Fluka. Zinc acetate [$(CH_3CO_2)_2Zn$] (99.99%) was purchased from Sigma-Aldrich. Fumed silica nanoparticles (SiO_2) under the trade name AEROSIL® 200 were supplied by Degussa AG (currently Evonik Industries) (Hanau, Germany). The nanoparticles had an average primary particle size of 12 nm, a specific surface area of 200 $m^2\,g^{-1}$ and a SiO_2 content >99.8%. All other materials and solvents used for the analytical methods were of analytical grade.

2.2. PET synthesis and in situ preparation of PET/SiO_2 nanocomposites

For the synthesis of PET, the reaction mixture comprised 31 g (0.50 mol) of EG, and 44.134 g (0.227 mol) of DMT ester (molar ratio of EG/DMT = 2.2), 50 ppm of $Zn(OCOCH_3)_2{\cdot}2H_2O$ as transesterification catalyst and 950 ppm of Sb_2O_3 as polycondensation catalyst.

The reaction mixture, in the transesterification step was heated to the final temperature (270 °C) under argon atmosphere, the stirring being at a constant speed (500 rpm). The reaction was completed after ≈3 h, when almost all the theoretical amount of methanol (18.4 mL) had been collected. In the second step (polycondensation) the catalyst Sb_2O_3 was added and a vacuum (4.0 Pa) was applied slowly (over about 30 min), in order to avoid excessive foaming and to minimize oligomer sublimation, which is a potential problem during melt polycondensation. During this time the excess of ethylene glycol was also, removed. The temperature remained stable at 270 °C while stirring speed was increased to 720 rpm. Polycondensation continued for about 1.5 h until the agitator speed decreased to 50–60 rpm, due to the increasing viscosity of the melt. After the polycondensation reaction was completed, the reaction tube was broken to get the product out of the tube. After the glass particles removal with a grinder, all polyester samples, were grounded in a mill, sieved, washed with methanol and dried at 110 °C for 12 h.

For the preparation of nanocomposites PET/SiO_2 containing 0.5, 1, 2, 3 and 4 wt% fumed SiO_2 nanoparticles, the same procedure was used as described before, while SiO_2 nanoparticles were added from the beginning of transesterification reaction.

2.3. Viscosity measurements

Intrinsic viscosity [η] measurements were performed with an Ubbelohde viscometer at 25 °C in a mixture of phenol and tetrachloroethane (60/40, w/w). The samples were maintained in the above mixture of solvents at 120 °C for 20 min to achieve complete solution. The solution was then cooled to room temperature and filtered through a disposable membrane filter (Teflon). The intrinsic viscosity of each sample was calculated using the Solomon–Ciuta [13] equation of a single point measurement:

$$[\eta] = [2(\eta_{sp} - \ln\,\eta_{rel})]^{0.5/c} \quad (1)$$

Some samples were partially insoluble in the above solvent mixture. In these samples the insoluble part was removed by filtration and washed extensively with the solvent mixture and acetone. After determination of the insoluble part, the new concentration of the solution was calculated and used in the Solomon–Ciuta equation for intrinsic viscosity calculation.

2.4. Differential scanning calorimetry (DSC)

The differential scanning calorimetric measurements were carried out with a Setaram DSC-141 calorimeter. Temperature and energy calibrations of the instrument were performed for different heating rates, using the well-known melting temperatures and melting enthalpies of high-purity zinc (Zn), tin (Sn) and indium (In) supplied with the instrument. Bulk-shaped specimens weighing about 6 mg were crimped in aluminium crucibles; an empty aluminium crucible was used as reference. The samples were heated from room temperature to 300 °C through their melting temperature T_m, with different heating rates. At this temperature, the samples remained for 5 min. Then, they were cooled to room temperature with the same rates. From these scans, the melting temperature (T_m), the melt-crystallization temperature (T_{mc}) of the samples, was measured.

2.5. Transmission electron microscopy

Electron diffraction (ED) and transmission electron microscopy (TEM) observations were performed on ultra thin film samples of the various nanocomposites prepared by an ultra-microtome. These thin films were deposited on copper grids. ED patterns and TEM micrographs were obtained using a JEOL 120 CX Electron Microscope operating at 120 kV. To avoid the destruction of the films with the exposure to the electron irradiation, an adequate sample preparation is required and for this reason, the thin films were coated with carbon black.

3. Theoretical background

Kinetic analysis of solid-state transformations is usually based on a single-step kinetic equation

$$\frac{d\alpha}{dt} = A\exp\left(-\frac{E}{RT}\right)f(\alpha) \quad (2)$$

where A (the preexponential factor) and E (the activation energy) are the Arrhenius parameters, R is the gas constant, α is the extent of conversion from the amorphous (liquid or solid) to crystalline phase and $f(\alpha)$ is the reaction model related to the mechanism. For non-isothermal conditions, $d\alpha/dt$ in Eq. (2) is replaced with $\beta(d\alpha/dT)$, where $\beta(=dT/dt)$, is the heating rate [14,15].

The ratio of the kinetic process $d\alpha/dt$ is proportional to the measured specific heat flow φ, normalized per sample mass (W/g):

$$\frac{d\alpha}{dt} = \frac{\varphi}{\Delta H_c} \quad (3)$$

where ΔH_c corresponds to the total enthalpy change associated with the crystallization process. The fractional extent of conversion α can be easily obtained by partial integration of non-isothermal thermal analysis curve.

The crystallization kinetics is usually interpreted in terms of the standard nucleation–growth model formulated by Johnson–Mehl–Avrami (JMA) [16–18]. This model describes the time dependence of the fractional extent of conversion α, usually written in the form:

$$\alpha = 1 - \exp[-(kt)^n] \quad (4)$$

where k is the Avrami crystallization rate constant, which is a function of temperature and in general depends on both the nucleation frequency and the crystal growth rate, and the Avrami kinetic exponent n is a parameter which reflects the nucleation frequency and/or the growth morphology [19]. It should be noted that both k and n are constants with specific values to a given crystalline morphology and type of nucleation for a particular crystallization condition [20] and that, based on the original assumptions of the theory, the value of the Avrami exponent n should be an integer ranging from 1 to 4. In this case, k and n are two adjustable parameters in order the data to be fitted. However, the use of Eq. (4) can still provide further insight into the kinetics of non-isothermal crystallization.

In the study of non-isothermal crystallization using DSC, the energy released during the crystallization process appears to be a function of temperature rather than time, as in the case of isothermal crystallization. In order to use Eq. (4) for the analysis of non-isothermal crystallization data obtained by DSC, it must be assumed that the sample experiences the same thermal history as designated by the DSC furnace. This may be realized only when the thermal lag between the sample and the furnace is kept minimal.

The Avrami rate equation can be obtained from Eq. (4) by differentiation with respect to time:

$$\left(\frac{d\alpha}{dt}\right) = k\eta(1-\alpha)[-\ln(1-\alpha)]^{1-1/n} \quad (5)$$

Eq. (5) is usually referred to as the JMA equation, and it is frequently used for the formal description of thermal crystallization data. It should be emphasized, however, that the validity of the JMA equation is based on the following assumptions: (a) isothermal crystallization conditions, (b) low anisotropy of growing crystals, (c) homogeneous nucleation or heterogeneous nucleation at randomly dispersed second-phase particles, and (d) growth rate of new phase controlled by temperature and independent of time.

A test for the applicability of the JMA model is based on the properties of the $y(\alpha)$ and $z(\alpha)$ functions (see below). Taking into account Eqs. (1)–(3), the kinetic equation for the JMA model can be written as

$$\varphi = \Delta H_c A\exp\left(-\frac{E}{RT}\right)f(\alpha) \quad (6)$$

where the function $f(\alpha)$ is an algebraic expression of the JMA model

$$f(\alpha) = n(1-\alpha)[-\ln(1-\alpha)]^{1-1/n} \quad (7)$$

The $f(\alpha)$ function should be invariant with respect to procedure parameters such as sample mass and heating rate for non-isothermal conditions. Malek [21–23] has shown that the functions $\varphi(t)$ and $\varphi(T)$ are proportional to the $y(\alpha)$ and $z(\alpha)$ functions that can easily be obtained by a simple transformation of DSC data. In non-isothermal conditions these functions are defined as follows:

$$y(\alpha) = \varphi\exp\left(\frac{E_c}{RT}\right) \quad (8)$$

$$z(\alpha) = \varphi T^2 \quad (9)$$

For practical reasons the $y(\alpha)$ and $z(\alpha)$ functions are normalized within the 0–1 range. The maxima exhibited by the $y(\alpha)$ and $z(\alpha)$ functions are defined as α_M and a_p^∞ respectively. The maximum of the $z(\alpha)$ function a_p^∞ is a constant for the JMA model ($a_p^\infty = 0.632$) and a characteristic "fingerprint" for it [21–24].

Table 1
Intrinsic viscosity, molecular weight, carboxyl end groups and insoluble content of the prepared nanocomposites.

Sample	$[\eta]$ (dL/g)	$\bar{M}_n$[a] (g/mol)	–COOH (eq/10^6)	Insoluble content (%)
PET	0.63	16,000	31	–
PET–0.5% SiO_2	0.74	20,500	26	–
PET–1% SiO_2	0.78	22,400	22	–
PET–2% SiO_2	0.69	18,500	25	–
PET–3% SiO_2	0.69	18,500	23	1.2
PET–4% SiO_2	0.64	16,500	20	3.7

[a] Molecular weights were measured using the proposed equation from Berkowitz $[\bar{M}_n] = 3.29\times10^4\times[\eta]^{1.54}$.

4. Results and discussion

4.1. Characterization of PET/SiO_2 nanocomposites

The average number of molecular weight of PET that is prepared according to the experimental procedure is about 16,000 g/mol. The prepared nanocomposites have slightly higher molecular weights, depending on the used silica amount. The highest molecular weight was achieved at low SiO_2 content (0.5 and 1 wt%) while at higher silica content the molecular weight was slightly reduced remaining higher of that of neat PET (Table 1). This behavior is because SiO_2 behaves as multifunctional additive due to its surface silanoil groups (–$Si(OH)_x$), as it was found from our previous studies [9,25]. These silanoil groups can react with hydroxyl end groups of PET macromolecules increasing its molecular weight and SiO_2 nanoparticles behave as chain extenders. However, at higher concentrations extended branched macromolecules are formed leading to crosslinked macromolecules, which can cause a slightly decrease in molecular weight. This is because the hydrodynamic dimensions of branched polymers in solution are smaller compared to those of linear polymers with the same molecular weight [26].

The same behavior can be found when organic compounds are used as multifunctional additives [27,28]. The formation of these crosslinked macromolecules, at SiO_2 content 3 and 4 wt%, was verified from the existence of insoluble fraction in phenol/tetrachloroethane solvent (Table 1).

Such a reaction between silica nanoparticles and a polyester was also reported in poly(butylene succinate) (PBSu) polyester and the

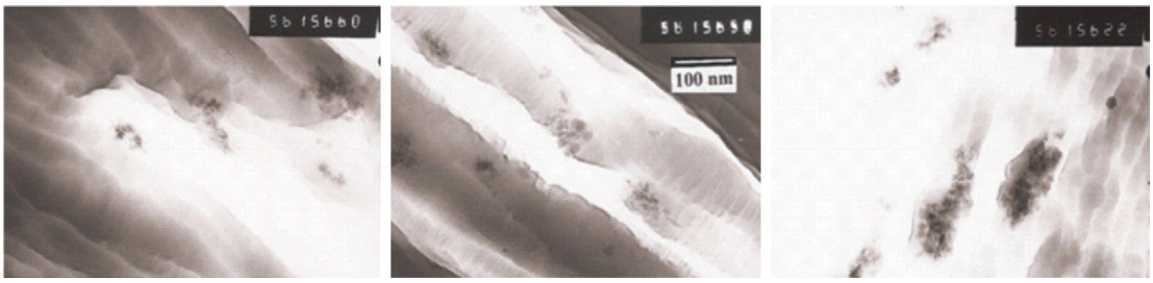

Fig. 1. TEM micrographs of PET/SiO_2 nanocomposites containing (a) 0.5 wt%, (b) 2 wt% and (c) 4 wt% SiO_2.

results of solid-state ^{29}Si NMR of PBSu/silica nanocomposites, as well as the results from FTIR spectra, indicated a covalent bonding between Si and the PBSu polymer backbone chain [29]. The existence of SiO_2 nanoparticles in PET matrix and the formation of branched and crosslinked macromolecules are expected to affect the thermal behavior and mainly the crystallization rates of PET. Of course, the crystallization behavior could, also, be affected from the nanoparticles dispersion into PET matrix and for this reason all samples were characterized using TEM (Fig. 1).

It is clear that small aggregates and individual nanoparticles appear in the samples, co-existing with larger agglomerates. This is typical in cases when such nanoparticles are dispersed in non-polar polymers, such as polyethylene and polypropylene. At the low concentrations of 0.5 till 2 wt% the filler exhibited better dispersion degrees with the agglomerate sizes being less than 100 nm. At the higher concentrations of 3 and 4 wt% some larger agglomerates, with maximum size of 200 nm, were observed. These agglomerates are formed due to the relatively strong interactions between the surface silanol groups of fumed silica and it seems that the reactions between the PET macromolecules are not sufficient to ensure the complete dispersion of the filler in the form of individual nanoparticles.

4.2. Thermal analysis

In order to understand the connection between silica particles content and crystallization in PET–SiO_2 nanocomposites, it is studied the crystallization behavior of the hybrid materials by means of DSC. Fig. 2 shows the melting peaks of all the as-prepared samples with a heating rate of 5 °C/min. As can be seen, at this temperature area, few of the samples present double melting peak with different overlapping percentage. This is clearer in samples containing more than 2 wt% SiO_2 nanoparticles and it must be depended on SiO_2 content. Furthermore, from Fig. 3 it is clear that the extent of overlapping in samples containing 2 wt% SiO_2 is dependent, also, on heating rate. The same behavior is also recorded for the sample containing 3 wt% SiO_2 while it was not easy to be observed in PET–4 wt% SiO_2, due to the great overlapping of the two peaks. In this figure it can be seen that as the heating rate is increased, the first peak is shifted to higher temperatures, while the second peak presents the opposite trend and shifts to lower temperatures. This is usual in polyesters due to the formation of crystals with different perfections [30–32].

Table 2
Melting temperatures, melting enthalpy and relative crystallinity of the as-prepared samples after heating with 5 °C/min.

Material	First peak T_m (°C)	Second peak T_m (°C)	Enthalpy ΔH (J/g)	Relative crystallinity (%)
PET	[a]	250.8	32.2	26.6
PET–0.5% SiO_2	[a]	251.1	27.8	20.0
PET–1% SiO_2	[a]	251.5	26.3	19.0
PET–2% SiO_2	246.5	253.6	27.7	20.2
PET–3% SiO_2	248.7	254.2	27.1	20.0
PET–4% SiO_2	[a]	250.7	28.8	21.4

[a] First melting peak can not be defined due to the overlapping.

The melting temperatures of the studied samples are presented in Table 2. The temperature of the main melting peaks of the PET–SiO_2 nanocomposites containing different SiO_2 contents, com-

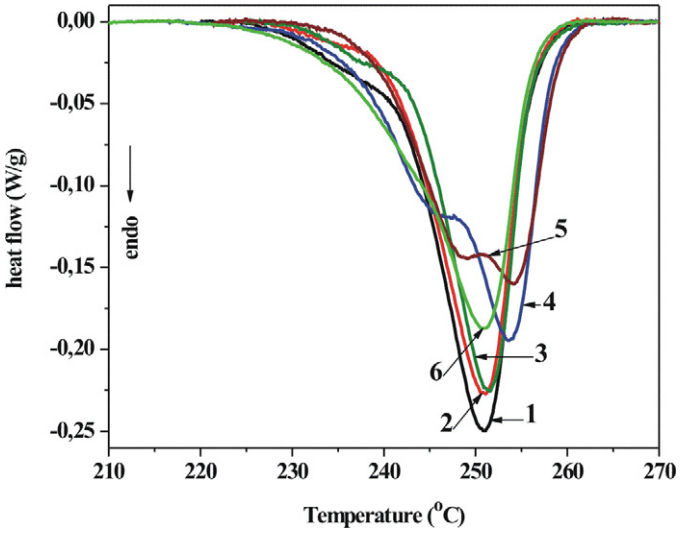

Fig. 2. Melting peaks of the studied samples with heating rate 5 °C/min. (1) PET, (2) PET–0.5% SiO_2, (3) PET–1% SiO_2, (4) PET–2% SiO_2, (5) PET–3% SiO_2 and (6) PET–4% SiO_2.

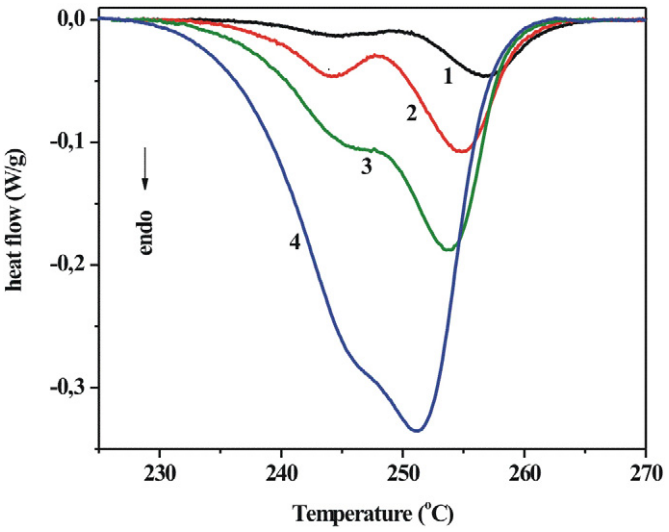

Fig. 3. Melting peaks of the PET–2% SiO_2 sample at different heating rates. (1) 1 °C/min, (2) 2.5 °C/min, (3) 5 °C/min and (4) 7.5 °C/min.

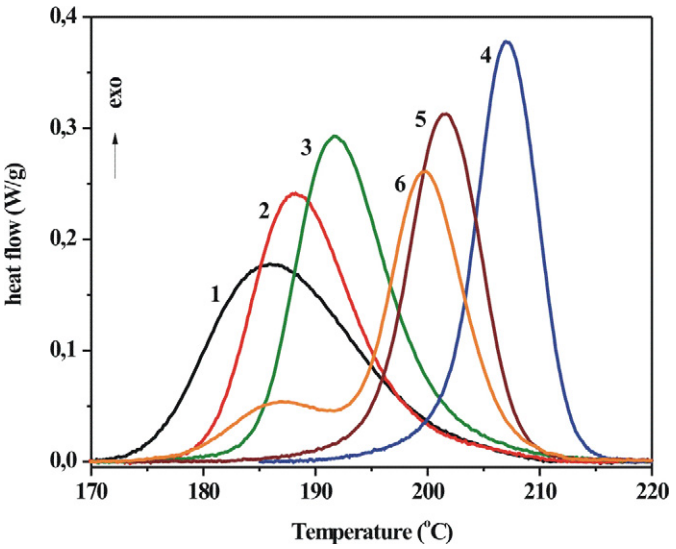

Fig. 4. Melt-crystallization exothermic peaks of all the studied samples during cooling, with cooling rate 5 °C/min. (1) PET, (2) PET–0.5% SiO_2, (3) PET–1% SiO_2, (4) PET–2% SiO_2, (5) PET–3% SiO_2 and (6) PET–4% SiO_2.

pared with that of neat PET, was increased slightly with the increase of the inorganic silica from 0 to 3 wt%, but was decreased for 4 wt%. The melting enthalpies (ΔH_m) of the nanocomposites were decreased, compared to pure PET, and remained almost unchanged regardless to the SiO_2 content. The temperature difference between the two peaks of melting is decreased with the increase of the SiO_2 content in the PET composites.The relative crystallinity X_c was calculated using the equation:

$$X_c = \frac{\Delta H_m}{(1-m)\Delta H_o} \times 100\% \quad (10)$$

where ΔH_m was calculated from the areas under the melting peak, m is the quantity of SiO_2 and ΔH_o is the melting enthalpy of 100% crystalline PET, which is according to the literature 140 J/g [33].

In Fig. 4 are shown the crystallization exotherms of all samples at cooling rate 5 °C/min. Compared with neat PET, it is obvious that the crystallization temperature of the PET–SiO_2 nanocomposites was increased with inorganic silica content. The increase can be attributed to the incorporation of effective nucleation agent SiO_2 and its satisfactory dispersion in the PET matrix. It is well known that the molecular chains of pure PET present higher inflexibility and less mobility. As a result, both crystallization rate and nucleation rate are very slow, corresponding to the low crystallization temperature. The incorporation of SiO_2 nanoparticles into the PET matrix, results in the enhancement of the crystallization rate of PET by providing large numbers of nucleation sites, in other words, SiO_2 nanoparticles induce a growth of crystalline layer around their surface.

The crystallization peaks of PET–3 wt% SiO_2 and PET–4 wt% SiO_2 samples shift to higher temperature values than neat PET, but lower than the PET–2 wt% SiO_2 nanocomposite. However, it would be expected, also, nanocomposites with 3 and 4 wt% SiO_2 content to have higher crystallization temperatures, or at least similar to the sample containing 2 wt% SiO_2 and not lower, as was recorded. This behavior could be attributed to the extended branched and crosslinked macromolecules that these sample have, thus decreasing the crystallization rate of PET. As was reported by Papageorgiou et al. [34] a systematic decrease in crystallization peak temperature was observed for a given cooling rate by increasing branching content, which is even lower from neat PET. However, in our samples having crosslinked macromolecules the crystallization temperature is higher than that of neat PET. So, it seems

Table 3
DSC results of melt-crystallization for the PET/SiO_2 nanocomposites with respect to the SiO_2 content, with cooling rate 5 °C/min.

Material	T_c (°C)	Enthalpy ΔH (J/g)
PET	186.0	35.9
PET–0.5% SiO_2	188.2	34.7
PET–1% SiO_2	191.6	34.2
PET–2% SiO_2	207.0	33.2
PET–3% SiO_2	201.6	32.0
PET–4% SiO_2	187–199.9	34.2

that at these samples there are acting two different mechanisms simultaneously: SiO_2 nanoparticles, which accelerate the crystallization rate of PET and branched-crosslinked macromolecules, which reduce the crystallization rate. Taking into account that crystallization temperature for the nanocomposites with 3 and 4 wt% SiO_2 nanoparticles is higher than that of neat PET, it can be concluded that the effect of silica nanoparticles is higher than that of the corresponding of branched-crosslinked macromolecules. The crystallization temperatures from the melt and the crystallization enthalpy values for all samples are collected in Table 3.

4.3. Crystallization kinetics

The evaluation of the effect of SiO_2 nanoparticles and the formed branched-crosslinked macromolecules on crystallization rate of PET crystallization kinetics proceeds in two steps. At the first step the activation energy is calculated independently of the reaction model and at the second step the crystallization mechanism is discussed. For the kinetic study non-isothermal measurements with different cooling rates are used.

In Figs. 5 and 6 the exothermic melt-crystallization peaks of PET–1 wt% SiO_2 and PET–4 wt% SiO_2 at different cooling rates are presented comparatively, while the data of the other samples are not shown for briefness. It is clear that the peak shifts to lower temperatures with increasing cooling rate, while at the same time the peak height is increased. An explanation could be, that at the lower heating rate, the molecular chains may have enough time to pack up in a unit cell and then their nuclei grew up more rapidly, while at the higher cooling rate PET molecular chains are too late to be arranged regularly or to form crystal nuclei so that they needed the greater supercool degree in order to be well crystallized. The area under the crystallization exotherm in the heat flow vs. time thermogram, that presents the total change of enthalpy during the

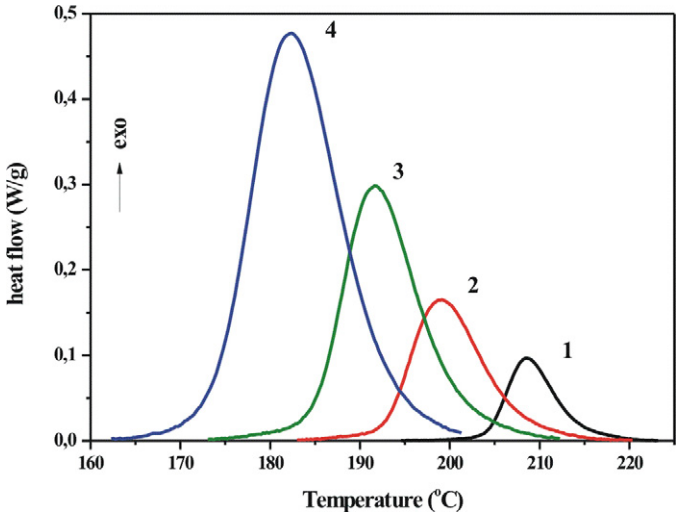

Fig. 5. Melt-crystallization exothermic peaks of the PET–1% SiO_2 sample at different cooling rates. (1) 1 °C/min, (2) 2.5 °C/min, (3) 5 °C/min and (4) 7.5 °C/min.

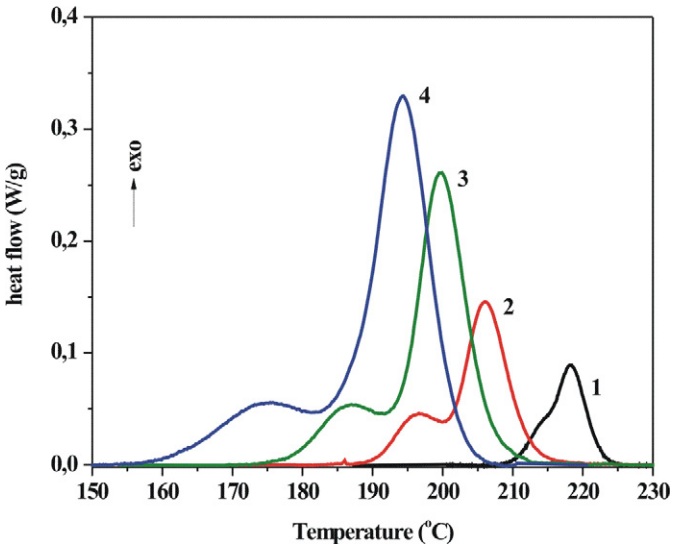

Fig. 6. Melt-crystallization exothermic peaks of the PET–4% SiO_2 sample at different cooling rates. (1) 1 °C/min, (2) 2.5 °C/min, (3) 5 °C/min and (4) 7.5 °C/min.

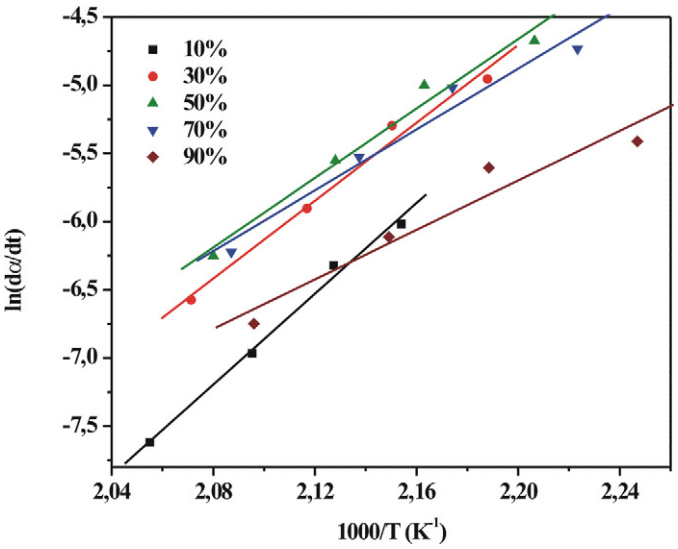

Fig. 7. Plot of $\ln(d\alpha/dt)$ vs. $1/T$ for melt-crystallization of PET–0.5% SiO_2.

crystallization, remains almost constant. The lower the cooling rate, the earlier the crystallization starts. It is noted that the PET/SiO_2 nanocomposites have higher peak temperatures than that of neat PET at all cooling rates. From Figs. 4 and 6 it can be seen that the PET–4 wt% SiO_2 sample, presents two distinct exothermic peaks. The first one that is displayed at higher temperature is shifted to lower temperatures and its height is increased with the increase of the cooling rate. The second one that is displayed at lower temperatures is shifted, also, to lower temperatures with the cooling rate increase, but its height remains unchanged. From the deconvolution of the overlapped crystallization peaks it is concluded that the ratio between the two populations (linear and branched molecules) remains constant for all the studied cooling rates. This behavior can be explained from the existence of branched and crosslinked macromolecules that this sample contains. It is well known that branched and crosslinked macromolecules are inhibiting the crystal formation of PET as it is increased the mean molecular weight of chains, thus resulting in the decrease of their mobility [25].

The Kissinger method is one of the most popular ways of evaluating the effective activation energy of non-isothermal polymer crystallization. However, Vyazovkin recently demonstrated [35–37] that this method provides invalid results when applied to the processes that occur on cooling such as melt-crystallization. Another limitation of the method is that it is applicable only to single-step processes where kinetics can be adequately represented by a single value of E. On the contrary, the crystallization rate is generally determined by the rates of two processes, nucleation and nuclei growth, where the activation energies are likely to be different. In this situation, the effective activation energy evaluated by using the Arrhenius equation should be a function of temperature, which makes a constant E estimated by Kissinger irrelevant. The popular integral isoconversional methods of Ozawa, Flynn and Wall are likely to be inapplicable to melt-crystallization because they require calculation of the logarithm of the heating rate, which is negative for a cooling process, and the use of the absolute value may invalidate the calculations as was demonstrated [35] for the Kissinger method. These methods may be applicable to glass crystallization because it occurs on heating.

From the other two isoconversional methods, the advanced isoconversional [38], and the Friedman's methods, which can be used for the calculation of the Activation Energy of nanocomposites during cooling, the Friedman's [39] method has been used. This is a differential isoconversional method which is based on Eq. (2) that leads to:

$$\ln\left(\beta\frac{d\alpha}{dT}\right) = \ln A + \ln f(\alpha) - \frac{E}{RT} \quad (11)$$

For a constant α, the plot of $\ln(d\alpha/dt)$ vs. $1/T$ obtained from curves recorded at several cooling rates, should be a straight line whose slope gives the value of E. It is obvious from Eq. (11) that, if the function $f(\alpha)$ is constant for a particular value of α, then the sum $\ln f(\alpha) + \ln A/\beta$ is also, constant. From Fig. 7 it is clear that activation energy of PET–0.5 wt% SiO_2 sample depends on degree of conversion, since the straight lines are not parallel. The dependence of the activation energy on the degree of conversion is presented in Fig. 8 for all the studied samples. As it can be seen at all the plots the activation energy does not have almost the same value for all the area of crystallization conversion α, presenting a more or less higher trend to increase the E with α. PET/SiO_2 samples present lower activation energy compared to that of neat PET, except those of PET–4 wt% SiO_2, for a region of crystallization conversion. Also, in this sample

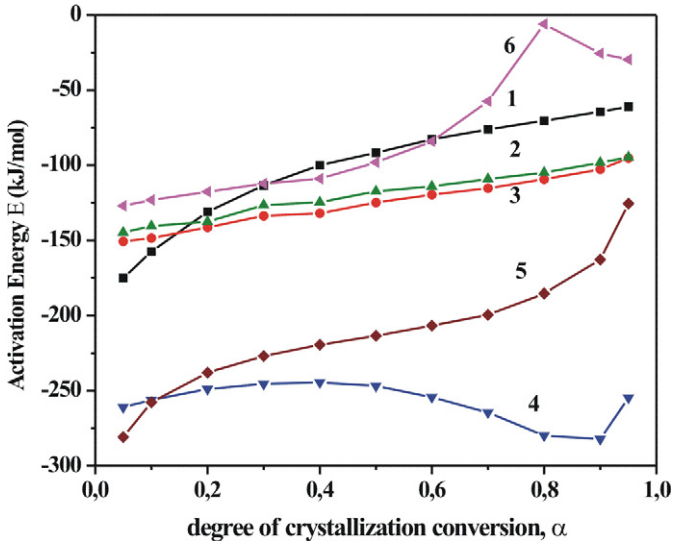

Fig. 8. Dependence of the activation energy (E) on the degree of crystallization conversion according to the Friedman's method. (1) PET, (2) PET–0.5% SiO_2, (3) PET–1% SiO_2, (4) PET–2% SiO_2, (5) PET–3% SiO_2 and (6) PET–4% SiO_2.

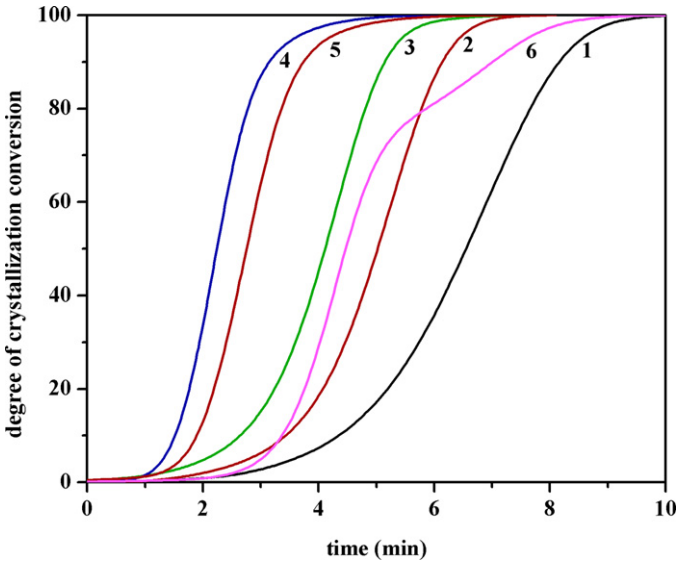

Fig. 9. Degree of crystallization conversion vs. time for melt-crystallization of all the studied samples, with cooling rate 5 °C/min. (1) PET, (2) PET–0.5% SiO_2, (3) PET–1% SiO_2, (4) PET–2% SiO_2, (5) PET–3% SiO_2 and (6) PET–4% SiO_2.

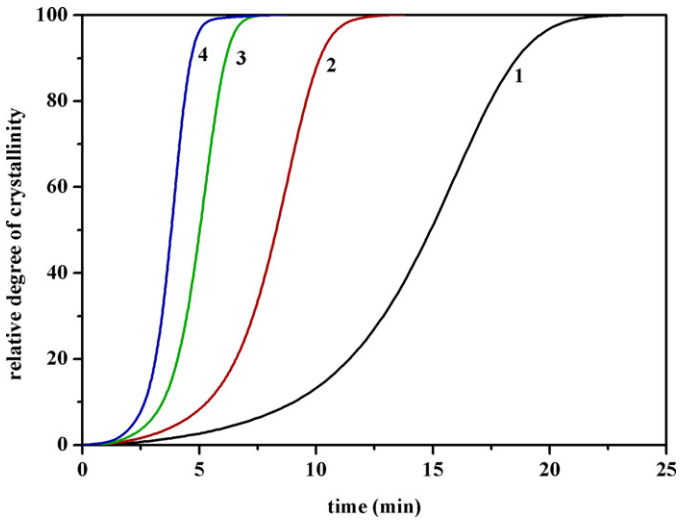

Fig. 10. Degree of crystallization conversion vs. time for melt-crystallization of PET–0.5% SiO_2 at different cooling rates. (1) 1 °C/min, (2) 2.5 °C/min, (3) 5 °C/min and (4) 7.5 °C/min.

the activation energy presents a maximum value for the crystallization conversion $\alpha = 0.8$ which could be attributed to the second overlapped crystallization peak. This dependence of E on α, is an indication of a complex reaction with the participation of at least two different crystallization mechanisms with different activation energies, which are taking place at different degrees of crystallization conversion. At low degree of crystallization conversion, SiO_2 has a more pronounce effect as it is required less activation energy, compared to the higher values, probably because in this region SiO_2 is stronger as a nucleation factor. There are only few works in the literature for the calculation of the activation energy of PET/SiO_2 nanocomposites. Wang et al. [7] calculated the activation energy using the Kissinger's, Augis-Bennet and Takhor methods and Ke et al. [12], also, with the Kissinger's method. In both works the conclusion was that the activation energy for PET is lower than for the studied PET/SiO_2 samples. The calculated values of the activation energy for PET samples from these works are different and the methods that have been used provide invalid results when applied to the processes that occur on cooling [35–37].

In order to obtain kinetic information, the experimental data such as those shown in Figs. 5 and 6 have to be presented in the form of the degree of crystallization conversion vs. time. Fig. 9 illustrates the degree of crystallization conversion α as a function of time of all the studied samples at cooling rate 5 °C/min. For a given cooling rate (5 °C/min), the curves of the degree of crystallization conversion vs. time show that for all the samples the time needed in order the crystallization process to be completed is decreased, compared to that of PET. For the samples with higher contents of SiO_2 (PET–3% SiO_2, PET–4% SiO_2), the completion time of crystallization is increased again compared to that of PET–2% SiO_2. In the literature there are few articles concerning the effect of SiO_2 on PET. In these articles it can be seen that SiO_2 enhance the crystallization rate of PET, by increasing the amount of SiO_2 [6,10] and that for content higher than 2 wt% the crystallization temperature of PET–3% SiO_2 and PET–4% SiO_2 nanocomposites is smaller than PET–2% SiO_2 nanocomposite, as shown in Table 3.

The curves of α vs. time (t) at four different cooling rates for PET–0.5% SiO_2 samples, non-isothermally crystallized, are plotted in Fig. 10, as an example showing that as the cooling rate is increased, the crystallization time is decreased. The same conclusion applies for PET and all the other nanocomposites. PET–4% SiO_2 sample presented a clearly different behavior. Initially, the degree of crystallization conversion increases exponentially till about 70% and then its slope is changed due to the second overlapping crystallization peak.

For the kinetic description of polymer's crystallization, as it has been mentioned previously, Avrami model is used. A first method for the examination of the JMA model's applicability is the linearity of the Avrami plot. Eq. (5) can be arranged as follows by taking its double logarithm

$$\log(-\ln(1-\alpha)) = n \log t + \log k_A \quad (12)$$

where k_A is the composite Avrami rate constant ($k_A = k^n$). The plots of $\log(-\ln(1-\alpha))$ vs. $\log t$ obtained from curves recorded at several cooling rates, should be straight lines and their slope gives the value of n. Nevertheless, it is well known that a double logarithmic function, in general, is not very sensitive to quite small changes to its argument. Therefore, it can be expected to observe substantial linearity in the plots of $\log[-\ln(1-\alpha)]$ vs. $\lg t$ even in the case that the JMA model is not fully fulfilled.

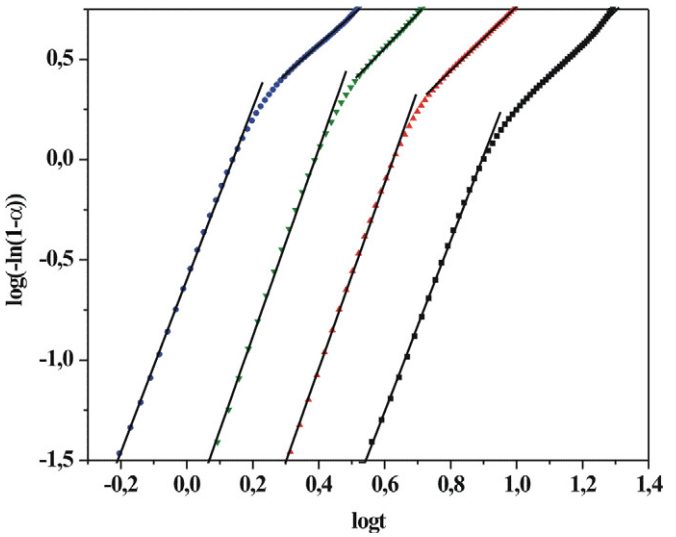

Fig. 11. Avrami plot for melt-crystallization of PET–2% SiO_2 at different cooling rates. (1) 1 °C/min, (2) 2.5 °C/min, (3) 5 °C/min and (4) 7.5 °C/min.

Table 4
Avrami exponent's n for melt-crystallization for all PET/SiO_2 nanocomposites.

Samples	Rate (°C/min)	n_1	n_2
PET	1	5.8	–
	2.5	5.0	–
	5	4.4	–
	7.5	4.7	–
PET–0.5% SiO_2	1	5.6	4.6
	2.5	5.3	4.4
	5	5.7	4.9
	7.5	5.9	4.8
PET–1% SiO_2	1	5.5	2.0
	2.5	5.5	2.3
	5	4.9	2.0
	7.5	4.1	2.4
PET–2% SiO_2	1	4.3	1.6
	2.5	4.6	1.6
	5	4.7	1.7
	7.5	4.3	1.5
PET–3% SiO_2	1	4.9	2.2
	2.5	4.6	1.5
	5	4.2	1.6
	7.5	3.5	1.9

In Fig. 11 is shown the double logarithmic plot of $\log[-\ln(1-\alpha)]$ vs. $\log t$ for PET–2% SiO_2 nanocomposite, at various cooling rates. PET samples present a linear area as Gao et al. had already presented [40] and the calculated values for the Avrami exponent are in the range of the literature data. As the content of SiO_2 is increased the first linear portion, is followed by a deviation at longer times which is increased as the quantity of the SiO_2 is increased. Usually, this deviation is considered to be due to a secondary crystallization, which is caused by the spherulite impingement in the later stage. The linear portions are almost parallel to each other, shifting to a shorter time with increasing β, indicating that the nucleation mechanism and crystal growth geometries are similar for the primary and secondary crystallization at all cooling rates. Each region takes place at a different degree of crystallization PET/SiO_2 and gives different values for n (n_1 and n_2). The PET–4% SiO_2 sample presents a little different behavior due to the two overlapping peaks exhibiting large overlapping area between the areas of the two peaks. So, for this sample is not easy to distinguish for each crystallization peak the two crystallization mechanisms and the Avrami exponents have not been calculated.

The values of Avrami exponents n_1, n_2, are presented in Table 4. In all the studied samples, the secondary crystallization presents lower value of the Avrami exponent, compared to the first crystallization for every value of β ($n_2 < n_1$—Table 4). This could be connected with the gradual increase of the influence of branched and crosslinked macromolecules. So, it becomes clear that the presence of SiO_2 nanoparticles in PET, drastically modifies the crystallization mechanism of the nanocomposites, as it was clear from the activation energy measurements. This may be due to the predominant nucleation activity of the SiO_2 in PET. But all the percentage contents of SiO_2 examined are effective as heterogeneous nuclei, a fact supported by the higher nucleation activity of PET/SiO_2. The higher effectiveness of SiO_2 heterogeneous nuclei can, also, be supported by comparing the T_o and T_p values of PET–SiO_2, that are always higher than that of PET nanocomposites at the corresponding cooling rates.

The non-isothermal crystallization kinetics of polymers has been described, also, by Ozawa theory [2,41] which can be considered as based on Avrami theory. Ozawa modified the Avrami equation for non-isothermal treatment, assuming that the polymer melt was cooled at a constant rate and the mathematical derivation of Evans [42,43] was valid. According to Ozawa theory the degree

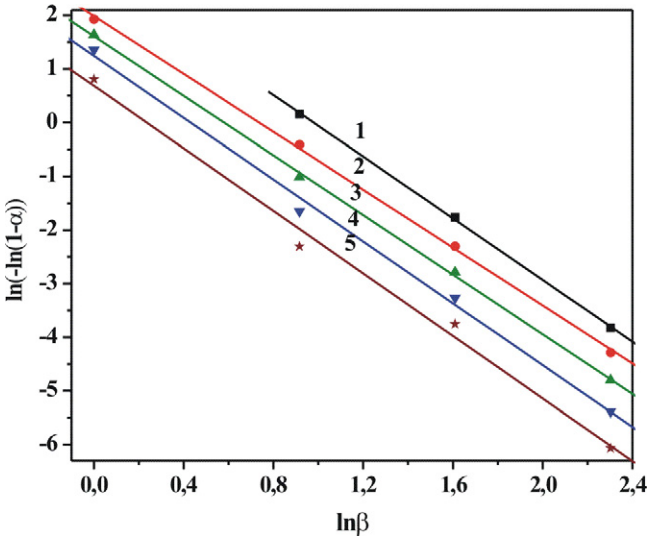

Fig. 12. Ozawa plots for non-isothermal melt-crystallization of PET–1% SiO_2 at different temperatures. (1) 198 °C, (2) 200 °C, (3) 202 °C, (4) 204 °C and (5) 206 °C, with fitting curves.

of conversion α at a temperature T can be calculated as

$$1-\alpha = \exp\left(\frac{-k(T)}{\beta^m}\right) \quad (13)$$

where β is the cooling rate, m is the Ozawa exponent – which depends on the dimension of crystal growth – and $k(T)$ is the cooling crystallization function, which is related to the overall crystallization rate and indicates how fast the crystallization occurs. Eq. (13) can be written as

$$\ln[-\ln(1-\alpha)] = \ln k(T) - m\ln\beta \quad (14)$$

If the above equation correctly describes the kinetics of non-isothermal crystallization, plots of $\ln[-\ln(1-\alpha)]$ vs. $\ln\beta$ should give straight lines and kinetic parameters $k(T)$ and m should be obtainable from the intercepts and slopes of the lines, respectively. For PET–1% SiO_2 and PET–3% SiO_2 nanocomposites the Ozawa plots of $\ln[-\ln(1-\alpha)]$ vs. $\ln\beta$ are shown in Figs. 12 and 13, respectively. As it can be seen, straight lines are obtained for PET–1% SiO_2 sample

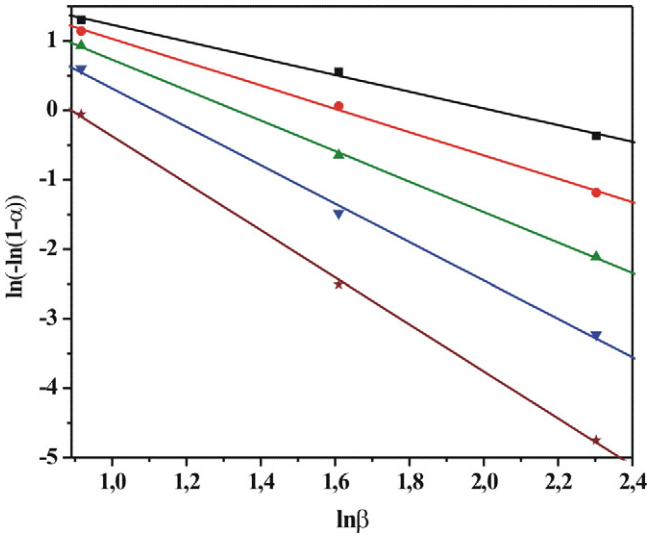

Fig. 13. Ozawa plots for non-isothermal melt-crystallization of PET–3% SiO_2 at different temperatures. (1) 198 °C, (2) 200 °C, (3) 202 °C, (4) 204 °C and (5) 206 °C, with fitting curves.

Table 5
Ozawa' s exponent m for melt-crystallization for all studied samples.

T (°C)	PET	PET–0.5% SiO_2	PET–1% SiO_2	PET–2% SiO_2	PET–3% SiO_2	PET–4% SiO_2
198	2.2	2.6	2.9	–	1.2	–
200	2.1	3.1	2.7	–	1.7	1.9
202	2.1	3.0	2.8	–	2.2	2.1
204	2.4	3.0	2.9	–	2.8	2.5
206	2.8	3.0	2.9	–	3.4	3.4

which is parallel among them (Fig. 12) but, for PET–3% SiO_2 sample the lines are not parallel (among them) (Fig. 13), indicating the failure of the Ozawa model to provide an adequate description of crystallization in both PET and PET/SiO_2 nanocomposites.

Since Ozawa equation [44] ignored secondary crystallization the reason that the non-isothermal crystallization of PET/SiO_2 at the lower temperature regions, does not follow the Ozawa equation can be explained by that, at a given temperature, the crystallization processes at different cooling rates are at different stages, that is, the lower cooling rate process is toward the end of the crystallization process, whereas at the higher cooling rate, the crystallization process is at an early stage.

It is obvious that the values of the slopes for PET/0.5% SiO_2 and PET/1% SiO_2 are higher than the values of PET while for PET/3% SiO_2, PET/4% SiO_2 are both smaller at lower temperatures and bigger than the values of neat PET at higher temperatures. P. Supaphol et al. [45] with non-isothermal measurements of PET found that Ozawa exponent ranged from 1.7 to 2.1 within the temperature range of 170–90 °C and Wang et al. [7] that Ozawa exponent ranged from 2.4 to 2.7 (see Table 5). For the sample PET/2% SiO_2, for the exponent m calculation, have not been found temperature regions where four of three points are in the same line—with sufficient accuracy. Additionally, the lines that are assigned between only two points, give a wide range of m values, without physical meaning. This wide range of m values – to a smaller extent – is also found in samples with higher SiO_2 content. This discrimination must be connected to the presence of branched and crosslinked macromolecules, and has as a result from content 2 wt% and more, the phenomenon be more complex.

The calculated values for PET are in the same area with the data of the literature and as far as we know there are not any data for Ozawa exponent in the literature, for PET/SiO_2. The dependence of the activation energy on the degree of crystallization conversion, from the Avrami and Ozawa plots, is an indication that for the kinetic description of the melt-crystallization of PET/SiO_2 cannot be used only one mechanism which obeys to Avrami equation.

In order to increase the certainty regarding the applicability of the JMA model that arises from the above discussion, we used another test method introduced by Malek and calculated the peak position of the $z(\alpha)$ function (α_p^∞), for the different heating rates. As can be seen from Fig. 14 the peak position values the $z(\alpha)$ function, for the different heating rates, for sample PET–3% SiO_2, are far from the accepted area of values (0.63) for the $z(\alpha)$ function. For all the samples the average volume of the peak position of the $z(\alpha)$ function is: for neat PET $\alpha_p^\infty = 0.62 \pm 0.04$, for PET–0.5% SiO_2 $\alpha_p^\infty = 0.62 \pm 0.02$, for PET–1% SiO_2 $\alpha_p^\infty = 0.57 \pm 0.02$, for PET–2% SiO_2 $\alpha_p^\infty = 0.44 \pm 0.05$, for PET–3% SiO_2, $\alpha_p^\infty = 0.47 \pm 0.02$ and for PET–4% SiO_2, $\alpha_p^\infty = 0.39 \pm 0.02$. The bigger the content of SiO_2 nanocomposites, the more shifted of the peak of the $z(\alpha)$ to smaller α values, which mean that more and more is decreased the applicability of the JMA model. (With the higher content of SiO_2, the peak of $z(\alpha)$ is shifted to smaller values of α, this meaning that the applicability of the JMA model is decreased.) This is a strong indication that the melt-crystallization of PET/SiO_2 nanocomposites cannot be described by one kinetic mechanism which obeys to the Avrami model. It is clear that we have at least two different crystallization mechanisms. However, their study using more than one different mechanism is a mathematical and physical complicated problem especially for the crystallization during cooling and is out of the scope of the present paper.

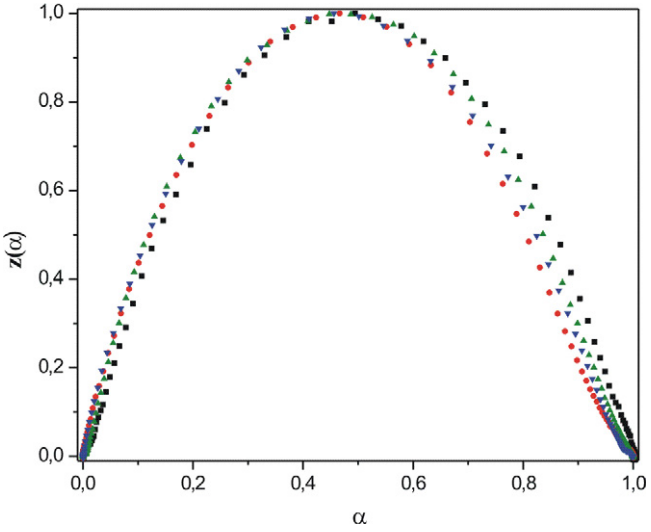

Fig. 14. Normalized $z(\alpha)$ function obtained by transformation of DSC data for different cooling rates for the melt-crystallization of PET–3% SiO_2.

5. Conclusions

Silica nanoparticles can act as multifunctional agents producing branched and crosslinked macromolecules by in situ polymerization of PET, when they are added at higher concentrations (over 2 wt%). This behavior has, also, affected the thermal properties of PET. The melting temperature of the nanocomposites was shifted slightly to higher temperatures by the addition of SiO_2 till 3 wt% while for PET–4 wt% SiO_2 nanocomposite the melting point was reduced. Also, the samples with SiO_2 more than 2 wt% present a double overlapped melting peak. As the amount of SiO_2 increases the crystallization became faster, shifting also the temperature of the crystallization peak to higher values, which are evidence that SiO_2 can act as nucleating agent. SiO_2 have high surface area, which in contact with PET matrix can induce a heterogeneous nucleation effect. All the samples present lower activation energy compared to that of neat PET, except those of PET–4% SiO_2. Extensive crystallization studies by using Avrami, Ozawa and Malek methods verified that PET and its nanocomposites must be crystallized by two mechanisms with different activation energies taking place in different degrees of crystallization.

References

[1] F. Pilati, M. Toselli, M. Messori, C. Manzoni, A. Turturro, E.G. Gattiglia, On specific factors affecting the crystallization of PET: the role of carboxyl terminal groups and residual catalysts on the crystallization rate, Polymer 38 (1997) 4469–4476.
[2] T. Ozawa, Kinetics of non-isothermal crystallization, Polymer 12 (1971) 150–158.

[3] V.L. Valev, C.D. Betchev, Calorimetric studies on stress-induced crystallization of pre-oriented poly(ethylene terephthalate) glasses, Thermochim. Acta 473 (2008) 50–53.
[4] H. Zheng, J. Wu, Preparation, crystallization, and spinnability of poly(ethylene terephthalate)/silica nanocomposites, J. Appl. Polym. Sci. 103 (2007) 2564–2568.
[5] W. Liu, X. Tian, P. Cui, Y. Li, K. Zheng, Y. Yang, Preparation and characterization of PET/silica nanocomposites, J. Appl. Polym. Sci. 91 (2004) 1229–1232.
[6] Y. Yang, H. Xu, H. Gu, Preparation and crystallization of poly(ethylene erephthalate)/SiO_2 nanocomposites by *in situ* polymerization, J. Appl. Polym. Sci. 102 (2006) 655–662.
[7] Y. Wang, C. Shen, H. Li, Q. Li, J. Chen, Nonisothermal melt crystallization kinetics of poly(ethylene terephthalate)/clay nanocomposites, J. Appl. Polym. Sci. 91 (2004) 308–314.
[8] A. Jeziorny, Parameters characterizing the kinetics of the non-isothermal crystallization of poly(ethylene terephthalate) determined by d.s.c., Polymer 19 (1978) 1142–1144.
[9] D. Bikiaris, V. Karavelidis, G. Karayannidis, A new approach to prepare poly(ethylene terephthalate)/silica nanocomposites with increased molecular weight and fully adjustable branching or crosslinking by SSP, Macromol. Rapid Commun. 27 (2006) 1199–1205.
[10] J.-P. He, H.-M. Li, X.-Y. Wang, Y. Gao, In situ preparation of poly(ethylene terephthalate)–SiO_2 nanocomposites, Eur. Polym. J. 42 (2006) 1128–1134.
[11] Y.-G. Zhu, Z.-Q. Li, D. Zhang, T. Tanimoto, Thermal behaviors of poly(ethylene terephthalate)/SiO_2 nanocomposites prepared by cryomilling, J. Polym. Sci. Part B: Polym. Phys. 44 (2006) 1351–1356.
[12] Y.-C. Ke, T.-B. Wu, Y.-F. Xia, The nucleation, crystallization and dispersion behavior of PET-monodisperse SiO_2 composites, Polymer 48 (2007) 3324–3336.
[13] O.F. Solomon, I.Z. Ciuta, Determination de la Viscosite Intrinseque de Solutions de Polymeres par une Simple Determination de la Viscosite, J. Appl. Polym. Sci. 6 (1962) 683–686.
[14] K. Chrissafis, G. Antoniadis, K.M. Paraskevopoulos, A. Vassiliou, D.N. Bikiaris, Compararive study of the effect of different nanoparticles on the mechanical properties and thermal degradation mechanism of in situ prepared poly(e-caprolactone) nanocomposites, Compos. Sci. Technol. 67 (2007) 2165–2174.
[15] K. Chrissafis, M.I. Maragakis, K.G. Efthimiadis, E.K. Polychroniadis, Detailed study of the crystallization behaviour of the metallic glass $Fe_{75}Si_9B_{16}$, J. Alloys Comp. 386 (2005) 165–173.
[16] M. Avrami, Kinetics of phase change I, J. Chem. Phys. 7 (1939) 1103–1112.
[17] M. Avrami, Kinetics of phase change II, J. Chem. Phys. 8 (1940) 212–224.
[18] M. Avrami, Granulation, phase change and microstructure—kinetics of phase change III, J. Chem. Phys. 9 (1941) 177–184.
[19] S. Vyazovkin, N. Shirrazzuoli, Isoconversional analysis of calorimetric data on nonisothermal crystallization of a polymer melt, J. Phys. Chem. B 107 (2003) 882.
[20] B. Wunderlich, Macromolecular Physics, Academic Press, New York, 1976 (Chapter 3) pp. 255–264.
[21] J. Malek, A computer program for kinetic analysis of non-isothermal thermoanalytical data, Thermochim. Acta 138 (1989) 337–346.
[22] J. Malek, The applicability of Johnson–Mehl–Avrami model in the thermal analysis of the crystallization kinetics of glasses, Thermochim. Acta 267 (1995) 61–73.
[23] J. Malek, Kinetic analysis of crystallization processes in amorphous materials, Thermochim. Acta 355 (2000) 239–253.
[24] K. Chrissafis, Th. Kyratsi, K.M. Paraskevopoulos, M.G. Kanatzidis, Crystal/glass phase change in KSb_5S_8 studied through thermal analysis techniques, Chem. Mater. 16 (2004) 1932–1937.
[25] D.S. Achilias, D.N. Bikiaris, V. Karavelidis, G.P. Karayannidis, Effect of silica nanoparticles on solid state polymerization of poly(ethylene terephthalate), Eur. Polym. J. 44 (2008) 3096–3107.
[26] B.H. Zimm, R.W. Kilb, Dynamics of branched polymer molecules in dilute solution, J. Polym. Sci. 37 (1959) 19.
[27] D.N. Bikiaris, G.P. Karayannidis, Synthesis and characterisation of branched and partially crosslinked poly(ethylene terephthalate), Polym. Int. 52 (2003) 1230–1239.
[28] M. Xanthos, C. Wan, R. Dhavalikar, P.G. Karayannidis, N.D. Bikiaris, Identification of rheological and structural characteristics of foamable poly(ethylene terephthalate) by reactive extrusion, Polym. Int. 53 (2004) 1161–1168.
[29] S.I. Han, J.S. Lim, D.K. Kim, M.N. Kim, S.S. Im, In situ polymerized poly(butylene succinate)/silica nanocomposites: physical properties and biodegradation, Polym. Degrad. Stabil. 93 (2008) 889–895.
[30] Y. Kong, J.N. Hay, Multiple melting behaviour of poly(ethylene terephthalate), Polymer 44 (2003) 623–633.
[31] I. Okazaki, B. Wunderlich, Reversible melting in polymer crystals detected by temperature-modulated differential scanning calorimetry, Macromolecules 30 (1997) 1758–1764.
[32] X.F. Lu, J.N. Hay, Isothermal crystallization kinetics and meeting behaviour of poly(ethylene terephthalate), Polymer 42 (2001) 9423–9431.
[33] J. Brandrup, E.H. Immergut, E.A. Grulke, A. Abe, D.R. Bloch, Polymer Handbook, 4th ed., Wiley, New York, 1999.
[34] G. Papageorgiou, D. Achilias, G. Karayannidis, D. Bikiaris, Isothermal and non-isothermal crystallization kinetics of branched and partially crosslinked PET DSC study, J. Therm. Anal. Calorim. 84 (2006) 85–89.
[35] S. Vyazovkin, Is the Kissinger equation applicable to the processes that occur on cooling, Macromol. Rapid Commun. 23 (2002) 771.
[36] S. Vyazovkin, N. Shirrazzuoli, Isoconversional approach to evaluating the Hoffman–Lauritzen Parameters (U^* and K_g) from overall rates of nonisothermal crystallization, Macromol. Rapid Commun. 25 (2004) 733.
[37] S. Vyazovkin, N.I. Dranca, Isoconversional analysis of combined melt and glass crystallization data, Macromol. Chem. Phys. 207 (2006) 20.
[38] S. Vyazovkin, Modification of the integral isoconversional method to account for variation in the activation energy, J. Comput. Chem. 22 (2001) 178.
[39] H.L. Friedman, Kinetics of thermal degradation of char-forming plastics from thermogravimetry. Application to a phenolic plastic, J. Polym. Sci. Part C 6 (1964) 183–195.
[40] Y. Gao, Y. Wang, J. Shi, H. Bai, B. Song, Functionalized multi-walled carbon nanotubes improve nonisothermal crystallization of poly(ethylene terephthalate), Polym. Testing 27 (2008) 179–188.
[41] J. Jabarin, Crystallization kinetics of polyethylene terephthalate. II. dynamic crystallization of PET, Appl. Polym. Sci. 34 (1987) 97–102.
[42] A. Duillard, P. Dumazet, B. Chabert, J. Guillet, A comparative model for anisothermal and isothermal crystallization of poly(ethylene terephthalate), Polymer 34 (1993) 1702–1708.
[43] U.R. Evans, The laws of expanding circles and spheres in relation to the lateral growth of surface films and the grain-size of metals, Trans. Faraday Soc. 41 (1945) 365–374.
[44] T.J. Ozawa, Kinetics analysis of derivative curves in thermal analysis, J. Therm. Anal. 2 (1970) 301–324.
[45] P. Supaphol, N. Dengseeyun, P. Srimoaon, M. Nithitanakul, Nonisothermal melt-crystallizationfor three linear aromatic polyesters, Thermochim. Acta 406 (2003) 207–220.